Interphase Development in a Three-Component Polymer System with Asymmetric Mobility

MARÍA DE LA PAZ MIGUEL,[1,2] J. PABLO TOMBA[1,2]

[1]Institute of Materials Science and Technology (INTEMA), National Research Council (CONICET), National University of Mar del Plata, Juan B. Justo 4302, 7600 Mar del Plata, Argentina

[2]Department of Chemical Engineering, Juan B. Justo 4302, 7600 Mar del Plata, Argentina

Received 1 October 2009; revised 4 December 2009; accepted 4 December 2009
DOI: 10.1002/polb.21931
Published online in Wiley InterScience (www.interscience.wiley.com).

ABSTRACT: We report a study on the interphase evolution in a system composed by three polymeric components with markedly different mobility distributed between two layers. One of the layers is a low-T_g blend containing a low molecular weight polystyrene (PS) as a plasticizer (low-M PS) and PS chains with much higher molecular weight (high-M PS). The counterpart is a high-T_g layer composed by polyphenylene oxide. The system was annealed at several temperatures between T_g of the polymer layers and the subsequent interphase development probed by optical sectioning with confocal Raman microspectroscopy. The profiles obtained revealed the existence of two diffusion fronts that advance in opposite directions, both showing a similar response with time and temperature. These fronts act as well-defined boundaries that structure the interphase into three well-defined regions with almost constant PS volume fraction. We discuss this particular phenomenology proposing a simple diffusion model that describes the main interphase features. © 2010 Wiley Periodicals, Inc. J Polym Sci Part B: Polym Phys 48: 627–633, 2010

KEYWORDS: confocal Raman microspectroscopy; diffusion; glassy polymers; interfaces; interphase evolution; oligomers; ternary system

INTRODUCTION Polymer diffusion plays a central role in the control of homogenization and phase separation, with implications in several technologies that depend critically on the properties of the interphases subsequently formed. Many diffusion problems in the polymers field can be well represented assuming that mass transport takes place in a binary system. However, there exist several practical situations that involve simultaneous transport of more than two chemical species and that require a more realistic description of the diffusion problem. Examples of the latter case can be found in membranes for separation processes,[1] coating technology, drug delivery systems,[2] or processing of polymer blends, among others.

The case of polymer diffusion in binary systems has been extensively studied, both experimental and theoretically. In a classic experiment, two molten polymers, nearly monodisperse, are brought into intimate contact and heated to promote mass transport across the original interface.[3] The classical Fickean formalism is used to describe the evolution of the interphase concentration profiles, through a single, in some cases concentration dependent, diffusion coefficient. The theoretical framework that describes the phenomenon predicts that the time scale for molecular transport depends on structural details of individual monomers, chain molecular weight, and interaction at the molecular level in the case of polymers chemically different.[4]

Diffusion in systems with more than two polymeric species, that is, multicomponent systems, appears practically and conceptually as a more complex problem. The topic embraces not only mass transport between chemically different components but also between polymer phases with wide distribution of molecular weights, either continuous or discrete (multimodal), where each molecular weight essentially behaves as a different component. When polymer diffusion proceeds in the dilute regime, that is, the polymeric species do not interact neither between them nor with the host matrix, the mass transport of each of the species is essentially independent and can be described by individual binary diffusion coefficients. In the concentrated regime, when all the components are present in appreciable amounts, individual fluxes appear coupled with the mass transport of the rest of the components. As a consequence, cross diffusion, that is, the motion of a given component as a result of gradients of other components, necessarily appears. The standard formulations for diffusion in multicomponent systems (Fickean, Onsager)[5] connect flows and driving forces linearly through phenomenological coefficients (diffusion or Onsager coefficients). In any of these formulations, the mass transport in a generic system with N components is described in terms of $N-1$ coupled diffusion equations, one material balance and $(N-1)^2$ coefficients.[6–8]

Correspondence to: J. P. Tomba (E-mail: jptomba@fi.mdp.edu.ar)
Journal of Polymer Science: Part B: Polymer Physics, Vol. 48, 627–633 (2010)

Mass transport in ternary polymer systems is a case with the complexity of multicomponent diffusion but amenable to analysis. Theoretical aspects of this topic, particularly related with the consistency of the aforementioned formulations, have been recently revisited by Vrentas.[9] In the polymer's field, some authors have drawn the attention to the potential of ternary system in providing new routes to control the interphase structure. For instance, a recent work of Aradian et al. analyzes theoretically the interphase development of a system formed by three polymers that are chemically different.[10] They show that, under certain conditions of chemical affinity between components, the interphase gives rise to a peculiar spatial structure composed by three well-defined layers with different chemical composition. Although the work is theoretical and only considers polymers with identical molecular mobility, it clearly shows the potential of multicomponent systems in providing spontaneous interphase layering at submicron scale.

This work presents an experimental study of interphase evolution in a model three-component polymer system. Our experimental design attempts to mimic a situation commonly found in practical applications where a plasticizer, confined in one polymeric phase is allowed to diffuse in a second one, also polymeric, but that differs markedly in physicochemical properties, that is, glass transition temperature (T_g) and chemical composition, from the first one.[11,12] One may imagine two possible situations: the plasticizer is originally confined in the phase of lower T_g or the opposite, that is, it migrates from the higher T_g phase. Here, we start considering the first of these cases. One of the phases is formed by a mixture of two polystyrene (PS) components (low-M/high-M), with strikingly different molecular weight, where the low molecular weight component plays the role of plasticizer. The components of that phase are chemically similar and were chosen to avoid segregation and further complications in the data analysis. The mixture is allowed to diffuse in a high molecular weight glassy polyphenylene oxide (PPO) matrix. The interphase that develops is probed by optical sectioning with confocal Raman microspectroscopy (CRM). This technique takes advantage of the natural spectroscopic contrast provided by the different chemical structures of PS and PPO and of the spatial discrimination at micron scale given by the confocal architecture. We analyze some of unusual aspects the interphase formed where the concept of bulk flow is invoked to explain the observed features. A simple diffusion model is introduced to qualitatively describe the interphase structure found.

EXPERIMENTAL

Materials Characterization

One low-M PS and two high-M PS samples with narrow molecular weight distributions ($M_w/M_n < 1.1$) were used, all of them purchased from Polymer Source (Dorval, Canada). The low-M PS component is characterized by $M_w = 740$ g/mol, $T_g = -5$ °C and will be also referred to as PS0.7. The high-M PS components are characterized by $M_w = 228{,}000$ g/mol, $T_g = 100$ °C and $M_w = 1.26 \times 10^6$ g/mol, $T_g = 102$ °C, and will be also referred to as PS200 and PS1000, respectively. A PPO sample from Aldrich ($M_n = 31{,}000$ g/mol, $M_w/M_n = 2.0$, $T_g = 212$ °C) was used as the glassy matrix. PPO was blended with 5% by weight of PS0.7 by freeze drying, to facilitate its processing; the resulting blend T_g was about 197 °C. Blends of low-M/high-M PS components, 7/3 by weight, were prepared by freeze-drying from benzene solutions; the T_g of the blend was about 25 °C. The oil used as immersion fluid (Cat. Nr. 11513859), with refractive index = 1.52, was provided by Leica. The glass transition temperatures of all the samples were measured with a Perkin-Elmer Pyris II DSC instrument, at a heating rate of 10 °C/min. Molecular weight data were provided by the manufacturer.

Sample Preparation for Diffusion Experiments

Cylindrical specimens (6.5 mm diameter) were prepared via sequential molding in a two-step process. The molding system operates under vacuum to avoid sample degradation. First, a thin film of PPO, about 100-μm thick, was molded at 40 °C above its T_g. Next, an aluminum guard ring was placed and secured on top of that film, at room temperature.[13] Finally, a thicker layer of the PS blend was vacuum molded on top of the PPO layer, in the cavity formed by the aluminum guard ring. The temperature of the second molding step was set to about 30 °C above the respective blend T_g, to minimize diffusion between layers at this stage. The PS layer was about 10 times thicker than the PPO layer to fulfill the condition of unlimited liquid supply, which simplifies the interpretation of the diffusion kinetics. These samples were annealed in a temperature-controlled oven (±0.5 °C) under dry nitrogen atmosphere for a period of time. They were then removed from the oven and quickly cooled to room temperature, which virtually stops interphase evolution, to be microscopically characterized.

Confocal Raman Microspectroscopy

Local Raman spectra were measured at room temperature on a Renishaw inVia Reflex confocal Raman microspectrometer equipped with a near infrared enhanced two-dimensional CCD detector (1024 × 256 pixels). The excitation source was Argon ion laser of 50 mW nominal power at 514 nm. The microscope objective used in the excitation and collection path was an immersion Leica ×100, with a numerical aperture (NA) of 1.3. A grating of 2400 lines/mm was used to set the spectral window in the shifts range between 500 cm^{-1} and 1500 cm^{-1}. The exposure time for each spectrum varied between 2 and 5 s with four accumulations. The best confocal performance is achieved operating the instrument in high confocality mode, which uses a combination of 3 pixels in the CCD camera with a slit width of 15 μm.

Figure 1 shows a scheme of the experimental setup. For optical sectioning, diffusion specimens were mounted on the automated microscope stage coupled to the Raman spectrometer. The vertical displacement of the stage (z-axis) is controlled by the instrument software (Wire 3.1). A drop of coupling oil was placed between the PPO layer and the microscope objective just before confocal Raman depth profiling was carried out. The oil matches the refractive

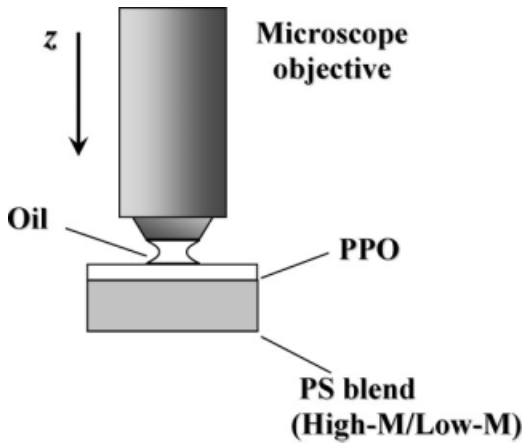

FIGURE 1 Experimental setup used for confocal Raman depth profiling.

index of the polymer phase minimizing laser refraction and distortions of the focal volume inside the sample. The oil was exhaustively removed with tissue paper before sample annealing. Optical sections were obtained at various distances from the PPO layer surface by moving the focal plane along the *z*-direction (see Fig. 1), resulting in a series of Raman spectra as a function of depth. The methodology used to obtain local concentration from the local Raman spectra has been described previously.[14] It takes about 20 min to acquire the whole concentration profile. The operative depth resolution for the aforementioned instrumental conditions ($\lambda = 514$ nm, $\times 100$ objective, high confocality), was 3 μm, as obtained by scanning in *z*-direction the intensity of the 520 cm^{-1} band of a silicon wafer immersed in the coupling oil.[13]

Computer Simulations

The set of second-order nonlinear coupled differential equations that describe the problem of transient diffusion in the ternary system was solved numerically using the MOLCH subroutine of the IMSL libraries (method of lines), in Fortran language.

RESULTS AND DISCUSSION

Confocal Raman Interphase Profiles

The characteristic Raman spectra of two of the components of the experimental setup, low-M PS and PPO, are shown in Figure 2, for the range of Raman shifts 500–1400 cm^{-1}. The Raman spectrum of the high-M PS sample is identical to that shown for the low-M PS. The spectral assignation has been discussed elsewhere,[15] but we see that the spectral profiles of PS and PPO are markedly different, which allows easy differentiation between these two components. Figure 2 also shows a Raman spectrum of a low-M PS/PPO = 1/1 by weight blend, where we see that the composite blend spectra is simply the addition of those of the pure components, and that they do not reveal significant shifting and/or broadening of Raman peaks due to PS-PPO interactions. The triplet centered at 1000 cm^{-1} is very sensitive to changes in PS/PPO composition, even though the method used to calculate this parameter uses the whole spectral range.[14]

Figure 3 shows a series of in-depth concentration profiles at the polymeric interphase in the form of volume fraction of PS (Φ^{PS}) versus depth, as probed by confocal Raman. The profiles were constructed by optically sectioning the composed system, starting from the PPO/coupling oil interface and by repeating measurements sequentially at deeper positions within the sample. Thus, the series of Raman spectra obtained were converted to local PS concentration via a calibration curve,[14] and these values plotted against the focusing depth, as read from the instrument software. The profiles shown in Figure 3 correspond to diffusion samples held at 120, 140, and 160 °C. There are some important features to note. First, at these temperatures, the PPO film remains in the glassy state in the course of the experiment, whereas the PS layer, composed by a mixture of low-M/high-M PS components in a 7/3 by weight ratio, is found as a liquid. Second, the experiment does not resolve the PS components individually as their Raman spectra are identical, that is, we measure global PS volume fractions. Finally, the range of depths accessible and shown by the figures is limited by the working distance of the microscope objective (210 μm). Although a major part of the PS layer, 1000-μm thick, is beyond the observational window, the most relevant details of the interphase evolution are well captured. The much larger thickness of the PS layer compared with that of the PPO was chosen to satisfy the condition of infinite liquid supply, that is, PS supplied from a source of invariant properties. As discussed in earlier work, this condition guarantees diffusion under nearly invariant driving forces simplifying the interpretation of the apparent diffusion kinetics.[16]

The shape of the PS concentration profiles shows some remarkable features. Originally, the boundary between PPO and PS was located at about 100 μm on the depth scale, dividing the PPO layer (0–100 μm) from the PS (100–1100 μm) side. As time increases, a complex interphase develops,

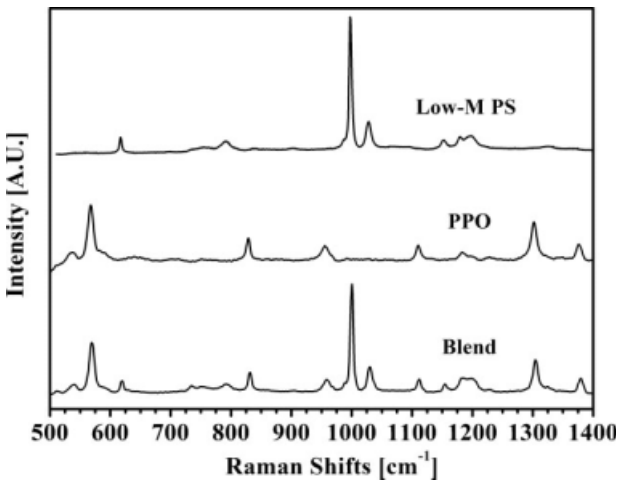

FIGURE 2 Raman spectra of individual components (low-M PS, PPO) and a 1/1 low-M PS/PPO homogeneous blend.

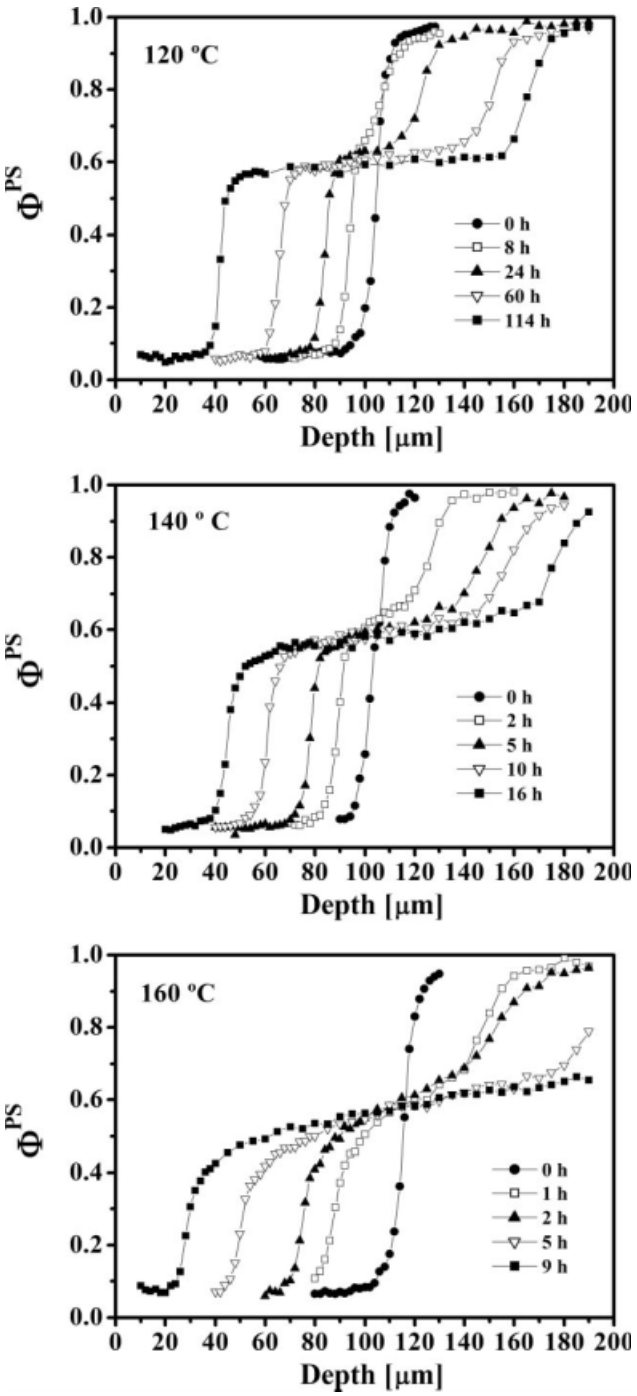

FIGURE 3 Typical depth profiles, in the form of PS volume fraction versus depth, obtained by confocal Raman. Annealing times and temperatures are specified in the legends.

showing as distinctive elements two abrupt transitions or diffusion fronts that advance in opposite directions. The first front advances toward the left (PPO side) evolving in the range of depths between 0 μm and 100 μm. The second front recedes with respect to the position of the original interface and can be seen at successive deeper positions in the range between 100 μm and 200 μm. These two diffusion fronts encompass a growing zone that we will refer to as plateau region, that is, the range of depths between both fronts.

The evolution of the first front indicates that PS has interdiffused with the PPO component. Overall, the PS profiles in the vicinity of this first front show a marked asymmetry, dropping off sharply in a narrow interval on the depth scale. They can be seen as a moving boundary limiting the PPO layer and what we called plateau region. These steep fronts, developed near a high T_g region (PPO layer) where diffusivity is expected to be markedly low, basically reflects the dramatic changes in molecular mobility experienced by the PS chains in the pathway from the liquid to the glassy side. On the scale of the spatial discrimination of our experimental technique, the diffusion fronts are indeed sharp, with no leading tails: the rounding observed at the profiles' edges entering to the glassy layer have a width in the order of the depth resolution of the technique. Previous work on liquid–glassy interphases has shown that this transition spans a region with dimensions on the order of the radius of gyration of the molecules of the glassy matrix.[16]

The plateau region is characterized by volume fractions of PS fairly constant, with spanned distances that increase with diffusion time. On average, Φ^{PS} throughout that region lies between 0.5 and 0.6, with a progressive leveling of the local slope as diffusion temperature decreases, that is, at 120 °C the PS profile is almost horizontal. Notice that the values of Φ^{PS} at the plateau are below the initial volume fraction of the low-M component in the PS layer, 0.7. The fact that the profiles are almost flat indicates that PPO molecules coming from the first region have been rapidly distributed throughout this second region, up the level of almost complete homogenization. This rapid distribution of PPO molecules in turn indicates a high level of plasticization of the plateau region, which is most likely due to a major presence of short low-M PS chains.

The second diffusion front appears dividing two polymer layers of nearly homogeneous composition, that is, the plateau region ahead and the pure PS layer behind. In this case, the front is somewhat less abrupt than that developed in the first region. Although one might anticipate the existence of this second front considering the marked difference in molecular weight between PS components, its backward motion appears at first sight surprising. The successive displacements shown by this front reveals the motion of an important part of PS molecules toward the right side, relative to the position of the original interface. These displacements of the second front appear in fine coupling with those of the first front in opposite direction.

Analysis of Front Kinetics and Interphase Features

Figure 4(A,B) presents plots of time evolution of front positions as a way of characterizing the interphase kinetics in the system of three components. The positions of both diffusion fronts for a given time were calculated from the maxima of the derivative curve of the PS concentration profile. Figure 4(A) shows results of advances of the first diffusion front

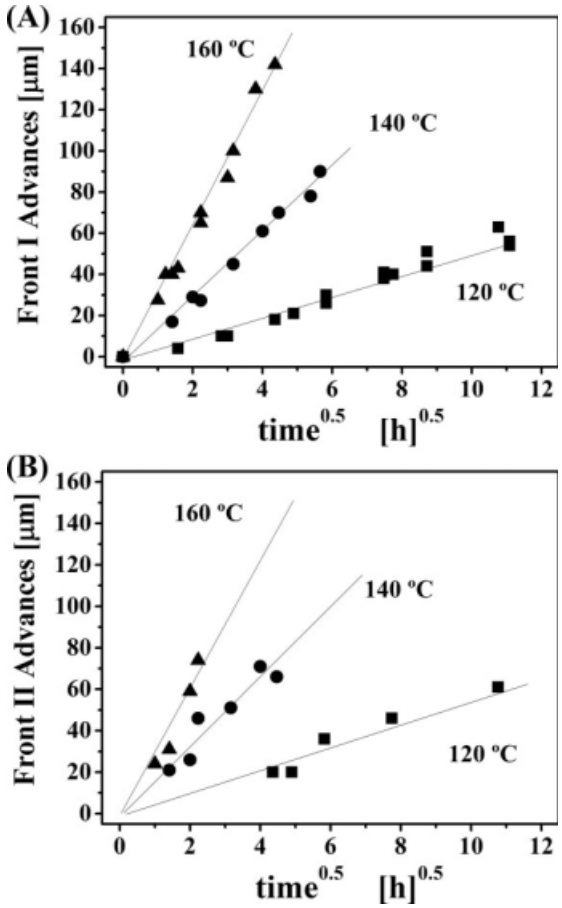

FIGURE 4 Advancing diffusion front kinetics plotted in Fickean fashion for several diffusion temperatures: (A) Advances of Front I; (B) advances of Front II. Data collected correspond to at least two independent samples by temperature. (A) also contains data taken from specimens with thicker PPO layers (200 μm).

(left-moving), presented in Fickean fashion, as a function of the square root of the elapsed diffusion time. We have also included data obtained from thicker PPO layers (ca. 200 μm thick), which allow the observation of larger advances of this front; see for instance, results at 160 °C for long annealing times. A representation of front advances as a function of diffusion time yielded a curve with a marked downward curvature, which rules out the possibility of a diffusion mechanism controlled by mechanical relaxation of the glassy matrix and characterized by a linear kinetics, that is, Case II, frequently found in diffusion of small penetrant molecules in glassy polymers. Despite the fact that the shapes of the profiles may resemble those found in Case II diffusion, that is, sharp diffusion fronts with a flat region behind, this mechanism is not expected to be operative for large sized penetrants, as the osmotic suctions generated by them are well-below the glassy matrix yield stress which precludes Case-II initiation.[17] As seen in Figure 4(A), all the front advances for the three temperatures are markedly Fickean, in agreement with previous work on the PS–PPO system.[16] We also see that temperature affects the rate of polymer diffusion in the usual way, that is, the higher the temperature the higher the diffusion rates.

Figure 4(B) shows the advances of the second front (right-moving) as a function of annealing time and temperature. The determination of the exact position is subjected to more uncertainty as the positions of the second front reached the limit of the experimental window (ca. 200 μm) for the longer diffusion times. We see that the advances of the second diffusion front toward the PS rich side also scale as $t^{1/2}$, an indication of Fickean transport. We also see that the rates of advance and the response to temperature are similar to those observed in the evolution of the first PS front.

To help us understand the mechanistic aspects of the interphase evolution, we investigate the influence of factors other than temperature or time on the diffusion kinetics. For instance, we paid attention to the role played by the high-M PS component in the interphase development, particularly on how this component operates on the mechanisms of advance of both diffusion fronts. With this idea, we carried out experiments in which the molecular weight of the high-M PS component was increased by about fivefold, using the PS1000 sample instead of PS200. Notice that the only difference between components is the molecular weight as the glass transition temperatures of both polymers are similar. We then redid the diffusion experiment at 140 °C, including the same amount of PS1000 than that used of PS200 in the original formulation. We observed that the PS profiles developed were not affected by this change and that they presented exactly the same features than those already described. The results of front kinetics are summarized in Figure 5, where we compare both experiments. The solid symbols represent the original results obtained with the PS200 sample, whereas open circles refer to those obtained with PS1000. We see that both PS fronts advanced with nearly the same rate; despite the fact, we increased the molecular weight of the high-M component by about five times.

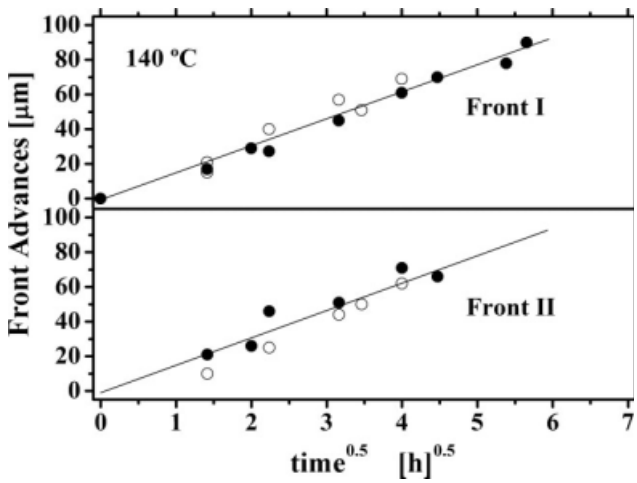

FIGURE 5 Comparison of advancing diffusion front kinetics between systems with different high-M components. Solid symbols: PS200 (M_w = 228,000 g/mol); open symbols: PS1000 ($M_w = 1.26 \times 10^6$ g/mol).

The observation on the apparent independence of front advances with the molecular weight of the high-M PS component suggests that the diffusion of the low-M PS component is the process that controls the mechanism of interphase development. In our view, interphase evolution begins when the low-M PS component diffuses toward the PPO side in Fickean fashion, generating the first diffusion front. The phenomenology of this liquid–glassy diffusion process has been analyzed in detail by us and other authors, see refs. 17 and 18 for further details. As the intrinsic diffusivities of PS and PPO components are markedly different (see below), this low-M PS diffusion generates a pressure gradient on the PPO side. To maintain a homogeneous density in this part of the system, the pressure gradient relaxes by bulk flow in, opposite direction, that is, toward the right side. Bulk flow is an expected feature in polymer pairs with asymmetric mobility, as established by elegant experiments made by Kramer and coworkers.[19] Kramer and coworkers followed the displacements of inert markers in polymer couples with asymmetric mobility, that is, two PS samples with markedly different molecular weight. Their experiments showed conclusively that the displacement of markers, which reflect the motion of the system as a whole, occurs toward the side of the faster moving species. In our system, this bulk flow drags all the species toward the PS side, appearing superposed with the rest of diffusive fluxes. As the molecular weight of the high-M PS is much larger than that of low-M PS, high-M PS does not contribute significantly to mass transport toward the PPO side, remaining essentially as a concentration step that moves backward by the effect of bulk flow. To us, this picture would explain the existence and evolution of the second PS front and the dynamics of the whole interphase.

The fact that the relative motions of both fronts are coupled and have similar responses to time and temperature seems consistent with this mechanism. Another possibility to explain the observed interphase development is that the second front originates from the segregation between low-M PS and high-M PS by virtue of the presence of initiator groups attached to the ends of the low-M PS chains. This segregation would also lead to the progressive shrinking of the PS layer, but, in this case, with markedly different temperature dependence than that observed in the motion of the first diffusion front: the evolution of the first front is controlled by the PS-PPO dynamics, entirely different to PS-PS dynamics.[20] Clearly, this is not the situation observed here.

Qualitative Modeling of the Interphase Structure

To further support our ideas on how the interphase evolves, we carried out computer simulations with a basic diffusion model that accounts for bulk flow contributions. From the many approaches that describe diffusion in multicomponents, we have chosen for familiarity the classic description where individual fluxes are written as linearly related with concentration gradients, that is, generalized Fickean formalism.

$$J_i = -D_i \nabla\Phi_i \quad i = 1...3 \tag{1}$$

where D_i will be referred to as intrinsic diffusivities, and expected to be variable as a function of the local environment. We assume that the net global flux with respect to laboratory coordinates is a superposition of intrinsic diffusion plus mass transported by the bulk flow mechanism.[21] In this way, the total flux of a given component is a superposition of its intrinsic diffusivity (first term) plus a contribution by bulk flow (second term):

$$J_i^T = J_i + \Phi_i \sum_j D_j \nabla\Phi_j \tag{2}$$

This expression further simplifies if we consider that the intrinsic diffusivity of the low-M PS is much larger than those of high-M PS and PPO. As a first factor, the monomeric friction coefficient of the PPO unit is much larger (by 1–2 orders of magnitude) than that of the PS unit.[20] In addition, molecular weights between components differ markedly. Among all the species present in the system (PPO, high-M PS, low-M PS) the low-M PS component is by far the most mobile. Under this condition, the bulk flow is essentially controlled by the component with the highest mobility. For a system of three components and diffusion in one dimension (x, equivalent to the z axis of the microscope), we have to solve

$$\frac{\partial\Phi_1}{\partial_t} = \frac{\partial}{\partial x}\left(D_1 \frac{\partial\Phi_1}{\partial x} - \Phi_1 D_1 \frac{\partial\Phi_1}{\partial x}\right) \tag{3}$$

$$\frac{\partial\Phi_2}{\partial_t} = \frac{\partial}{\partial x}\left(-\Phi_2 D_1 \frac{\partial\Phi_1}{\partial x}\right) \tag{4}$$

where 1 refers to low-M PS and 2, 3 to high-M PS and PPO, respectively. Notice that the whole set of equations is governed by a single diffusivity D_1, expected to be highly dependent on local concentration of all the species and temperature for our system. To keep the scheme simple and to avoid further complications arising from the rather complex dependency of D_1 with

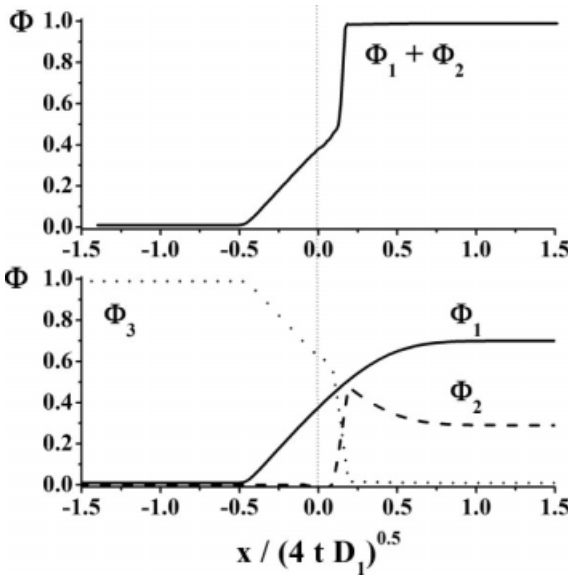

FIGURE 6 Numerical prediction of volume fraction profiles computed from the diffusion model. The top panel shows ($\Phi_1 + \Phi_2$), which is equivalent to the global PS volume fraction measured by confocal Raman. The bottom panel shows individual profiles for the three species.

local environmental properties, we solved the problem assuming that D_1 is a constant. Boundary conditions of no-flow were used for all the components. Initial conditions were consistent with the experiments carried out here: a 0.7/0.3 mixture of 1 and 2 components on the right side of the couple against a pure phase of component 3 on the left. Figure 6 shows the predicted concentration profiles in the three-component polymer system with the characteristics mentioned earlier. As the evolution in time of individual profiles are self-similar, results are presented as a function of the reduced variable $x/(4\ t\ D_1)^{0.5}$.

The top panel in Figure 6 shows the global PS concentration ($\Phi_1 + \Phi_2$) predicted by the model. We see that the calculated profiles present similar features to those found in the experiments: a first PS front advancing toward the PPO side and a second front that recedes. The fact that the Φ^{PS} value where profile crossovers the original interface and that the shape of the first advancing front are different to those experimentally observed is due to the simplistic assumption of constant D_1. For the same reason, the model does not predict the extended Φ^{PS} plateau observed in the experimental data, which originates in the dramatic changes in molecular mobility experienced for PS chains along the diffusion path. The development of a detailed model that accounts with detail the complex dependence of D_1 with Φ_i is underway.

The bottom panel shows individual profiles for the three species involved. One interesting prediction of the model is the enrichment of the high-M PS component (Φ_2) in the proximity of the second diffusion front, giving rise to a peaked profile. This enrichment that originates in the differential molecular mobility between PS species reveals another level of interphase structuration, that is, high-M PS chains would preferentially locate in the region close to the second diffusion front. This detail is overlooked here as we measure global PS composition, but it could be resolved using for instance a deuterated high-M PS to enhance the spectral contrast between PS species. We have particularly avoided at this stage of the project the use of deuterated species, considering that possible problems of segregation between components, that is, dPS-PPO or even between PS species considering the greater influence of ends groups of low-M PS chains, might complicate modeling and data interpretation. However, this option will be investigated in the future giving the higher level of detail on interphase structure that can be obtained with this strategy.

CONCLUSIONS

We have studied the interphase development in a model system of three components with markedly different mobility. We have seen that a combination of strikingly differential mobility between polymer species initially located in the same phase and concentration-dependent polymer diffusion, induces interphase structuration into three well-defined regions with almost constant PS volume fraction. From a mechanistic point of view, the interphase develops by initial diffusion of the low-M PS component in the high T_g phase, evolving as a sharp diffusion front that leaves a region with nearly constant PS concentration behind. This diffusion of the low-M PS component induces bulk flow in opposite direction giving rise to a backward motion of the original interface. This phenomenology is possibly a common feature in systems containing a plasticizer/low molecular weight additive that migrates between two polymer phases, a situation frequently found in several applications. Although our work was originally conceived with a different purpose, it confirms predictions advanced by Aradian et al. about the peculiar interphase development that systems with three polymeric components may offer.

This work was funded by ANPCYT (PICT06-1359). The confocal Raman microscope was acquired with funds from ANPCYT and CONICET (PME06-2170).

REFERENCES AND NOTES

1 Paul, D. R. J Membr Sci 2004, 241, 371–386.

2 Kumar, M. N. V. R.; Kumar, N.; Domb, A. J.; Arora, M. Adv Polym Sci 2002, 160, 45–117.

3 The case of diffusion of small gas or liquid molecules in a solid polymer can also be part of this discussion.

4 Composto, R. J.; Kramer, E. J.; White, D. M. Macromolecules 1988, 21, 2580–2588.

5 The Maxwell-Stefan formalism relates concentration gradients as linear combinations of individual fluxes.

6 Curtiss, C. F.; Bird, R. B. Ind Eng Chem Res 1999, 38, 2515–2522.

7 Fornasiero, F.; Prausnitz, J.; Radke, C. Macromolecules 2005, 38, 1364–1370.

8 Buxton, G. A.; Clarke, N. Macromolecules 2005, 38, 8929–8938.

9 Vrentas, J. S.; Vrentas, C. M. Ind Eng Chem Res 2005, 44, 1112–1119.

10 Aradian, A.; Saulnier, F.; Raphael, E.; de Gennes, P.–G. Macromolecules 2004, 37, 4664–4675.

11 Tomba, J. P.; Ye, X.; Lau, W.; Winnik, M. A. Polymer 2008, 49, 2055–2064.

12 Tomba, J. P.; Portinha, D.; Schroeder, W.; Lau, W.; Winnik, M. A. Colloid Polym Sci 2009, 287, 367–378.

13 Tomba, J. P.; Carella, J. M.; Pastor, J. M. Appl Spectrosc 2006, 60, 115–121.

14 Tomba, J. P.; De la Puente, E.; Pastor, J. M. J Polym Sci Part B: Polym Phys 2000, 38, 1013–1023.

15 Kuptsov, A. H.; Zhizhin, G. N.; Handbook of Fourier Transform Raman and Infrared Spectra of Polymers; Elsevier: Amsterdam, The Netherlands, 1998.

16 Tomba, J. P.; Carella, J. M.; Pastor, J. M. Macromol Chem Phys 2009, 210, 359–366.

17 Tomba, J. P.; Carella, J. M.; Pastor, J. M. Macromolecules 2009, 42, 3565–3572.

18 Lin, C. J.; Tsai, I. F.; Yang, C. M.; Hsu, M. S.; Ling, Y. C. Macromolecules 2003, 36, 2464–2474.

19 Green, P. F.; Palmstrom, C. J.; Mayer, J. M.; Kramer, E. J. Macromolecules 1985, 18, 501–507.

20 Composto, R. J.; Kramer, E. J.; White, D. M. Polymer 1990, 31, 2320–2328.

21 Crank, J. The Mathematics of Diffusion; Clarendon Press: Oxford, 1975.